Desalination and Water Treatment
www.deswater.com

doi: 10.5004/dwt.2017.21662

99 (2017) 204–210
December

Facile chemical bath deposition to fabricate RuO_2 electrodes for electrochemical chlorine evolution

Tran Le Luu[a], Jiye Kim[b], Jeyong Yoon[b,*]

[a]*Department of Mechatronics & Sensor Systems Technology, Vietnamese German University, Le Lai Street, Hoa Phu Ward, Thu Dau Mot City, Binh Duong Province, Vietnam*
[b]*School of Chemical and Biological Engineering, Seoul National University, Gwanak-gu, Daehak-dong, Seoul 151-742, Korea, Tel. +82 2 880 8941; Fax: +82 2 876 891; email: jeyong@snu.ac.kr*

Received 27 August 2017; Accepted 28 October 2017

ABSTRACT

Development of a facile preparation process for dimensional stable anodes (DSA) is an important issue to reduce the fabrication cost. During the last three decades, chemical bath deposition (CBD) has emerged as one approach which deposits a thin film with a facile method in ambient conditions. In this study, RuO_2 electrodes were fabricated by the CBD method for electrochemical chlorine evolution. The major results show that the CBD method enables the formation of uniform rutile RuO_2 nanocrystals with an average size of 30 nm. The electrode morphologies were formed with cracks and pores, and the RuO_2 thin films had good adhesion on the Ti substrates. Thermally treated RuO_2 films exhibited a high electrocatalytic activity and stability in chlorine evolution satisfying the requirements for a DSA. The amount of deposited RuO_2 as well as the cracks, electrocatalytic activity, and stability in chlorine evolution increased with the deposition time. CBD is an attractive synthesis route to fabricate a RuO_2 electrode for electrochemical chlorine evolution.

Keywords: Chemical bath deposition; RuO_2; Electro-catalyst; Chlorine

1. Introduction

RuO_2, which is one of the dimensional stable anodes (DSA), has been widely used in several fields such as the chlor-alkali industry, water electrolysis, oxygen reduction, organic synthesis, water treatment, electronics, and supercapacitors [1–4]. Especially, RuO_2 is a desirable electro-catalyst for chlorine and oxygen evolution due to its low overpotentials [5–7]. Although the RuO_2 electrode has an excellent catalytic property and reversibility, the low abundance and high cost of the Ru metal are major limitations to its commercial application [1–3]. It is well known that the physical and chemical properties of RuO_2 are strongly influenced by the synthesis routes [8]. RuO_2 can be synthesized by various methods such as thermal decomposition [9–11], sol-gel [12], electrostatic spray deposition [13], chemical vapor decomposition [14], electrodeposition [15], etc. However, it is desirable to develop a new simple process for the preparation of thin film RuO_2 electrodes to reduce their cost with a high production yield. Chemical bath deposition (CBD) has gained much attention over the last few years [16–18] because CBD is inexpensive, enables the facile synthesis of nanostructured thin films at low temperatures, and can be applied to large area deposition [19–26]. The low deposition temperature avoids oxidation or corrosion of metallic substrates and does not require a vacuum or applied potential at any stage as does chemical vapor deposition and electrodeposition [27–35]. To the best of our knowledge, up until now, CBD of RuO_2 for electrochemical chlorine evolution has not been studied yet. In this study, RuO_2 was synthesized with the CBD method for electrochemical chlorine evolution. The structures of the as-prepared electrodes were characterized

* Corresponding author.

with scanning electron microscopy (SEM), transmission electron microscopy (TEM), and X-ray diffraction (XRD). The electrochemical properties were examined by measuring the total chlorine concentration and by using cyclic voltammetry (CV), linear sweep voltammetry (LSV), and accelerated stability test (AST) methods.

2. Experimental setup

2.1. Electrode preparation

All chemicals were fine and high purity (99.7%) from Sigma-Aldrich, USA. Titanium foils (dimensions 30 × 20 × 0.25 mm) were polished with emery paper, degreased in acetone and etched in boiling hydrochloric acid (37 wt%) at 86°C for 60 min to produce a uniform roughness, and then used as the substrate. An acidic bath (pH = 2) was prepared with a mixture of 0.01 M $RuCl_3$ and 0.1 M NH_4Cl and stirred at 200 rpm. The chemical reactions (Reactions (i)–(iii)) in the bath can be represented as follows [27–35]:

$$RuCl_3 + 3H_2O \rightarrow Ru(OH)_3^+ + 3HCl \quad \text{(i)}$$

$$Ru(OH)_3^+ + NH_4Cl \leftrightarrow (NH_3)Ru(OH)_3^+ + HCl \quad \text{(ii)}$$

$$(NH_3)Ru(OH)_3^+ + n(OH)^- \rightarrow RuO_2.nH_2O\downarrow + NH_4OH + H^+ \quad \text{(iii)}$$

Slow hydrolysis of $RuCl_3$ occurs by heating in an acidic bath (Reaction (i)), and Ru hydroxide further reacts with NH_4Cl (Reaction (ii)). The Ti substrate was immersed vertically in the solution, and blackish colored particles started to precipitate on the Ti substrate (Reaction (iii)) when the bath temperature reached 60°C. Adsorption is a surface phenomenon due to the attractive force between the ions and substrate surfaces. After precipitation, the RuO_2 film was taken out of the bath, washed with DI water, and sintered for 1 h at 450°C in air conditions to remove the hydrous content [36]. The amount of RuO_2 nanoparticles deposited on the electrode surfaces was controlled by the deposition time and measured by the difference in the electrode weight (mg cm^{-2}) before and after the deposition [28].

2.2. Microstructure characterization

The microstructures of the electrode surfaces were characterized with field emission scanning electron microscopy (FE-SEM, JSM-6701F, JEOL Co., Japan). The SEM images were taken at a working distance of 7 mm with an accelerating voltage of 10 kV. The samples were positioned horizontally [37].

Crystal morphologies were examined with TEM (JEOL 2000EXII, Japan). The TEM samples were prepared by scraping off the coating using a sharp knife and dispersing the powders in isopropyl alcohol. A few drops of these solutions were deposited onto carbon film-coated Cu grids and analyzed with a microscope [38]. The accelerating voltage was 110 kV, the vacuum system was 10 Pa, and the tilting angles were ±25°.

To study the crystallinity of the RuO_2 electrodes, the high resolution XRD pattern was obtained with the grazing incidence technique on a D8 Discover (XRD, Bruker-AXS, Germany) diffractometer (CuKα, λ = 1.5406 Å). A scintillation counter detector scanned between 25° and 100° in 2θ with an angle of incidence of 0.5°, the working distance was 12 mm, and the accelerating voltage was 25 kV [39].

2.3. Electrochemical measurement

The electrochemical characterizations of the metal oxide electrodes were examined using CV and LSV measurements [40]. The experiments were performed at room temperature in a conventional single compartment cell with three electrodes using a computer-controlled potentiostat (PARSTAT 2273A, Princeton Applied Research, USA). The volume of the electrolyte was 150 mL. RuO_2 was used as the working electrode (anode), Pt (Samsung Chemicals, South Korea) as the counter electrode (cathode), and Ag/AgCl (in saturated KCl) as the reference electrode [41].

CV was measured in the 0.5 M H_2SO_4 electrolyte. The range of the scan rate was 5–320 mV/s. The CV curves were recorded over a range potential of 0–1 V vs. Ag/AgCl (KCl saturated). The electrochemical active surface area of the RuO_2 electrode was calculated by measuring the voltammetric charge (q) which indicates the number of electrochemical active sites [42]. The voltammetric charge (q) at 0–1 V vs. Ag/AgCl (KCl saturated) can be described by the pseudo-capacitive reaction (Reaction (iv)) which consists of coupled redox transitions with a broad reversible peak around 0.6 V vs. Ag/AgCl [42]:

$$RuO_x(OH)_y + zH^+ + ze^- \rightarrow RuO_{x-z}(OH)_{y+z} \quad \text{(iv)}$$

Total or outer active surface areas can be obtained by varying the scan rate of the applied potential. For example, the total active surface area, which includes both the inner and outer active surface areas, can be obtained at the low scan rate. On the other hand, the outer active surface area can be obtained at the high scan rate [42]. This is explained by the fact that both the inner and outer active surface areas can exchange protons with the solution at low scan rate while the inner active surface area fails to participate in this reaction at the high scan rate. Then, the total or outer active surface area can be estimated by extrapolating the voltammetric charge to an infinitely low (0) or high (∞) scan rate as in the following equations (Eqs. (1)–(3)) [42]:

$$q_{total} = q_{inner} + q_{outer} \quad (1)$$

$$q(v) = q_{outer} + A(1/\sqrt{v}) \quad (2)$$

$$1/q(v) = 1/q_{total} + B\sqrt{v} \quad (3)$$

where v is the scan rate; $q(v)$ is the voltammetric charge at the scan rate v; q_{total} is the voltammetric charge obtained at the infinitely low (0) scan rate; q_{outer} is the voltammetric charge obtained at the infinitely high (∞) scan rate; q_{inner} is related to the voltammetric charge of the inner surfaces, and A and B are constants.

LSV measurements were conducted in electrolytes containing 5 M NaCl + 0.01 M HCl (pH = 2) which are favorable

conditions for chlorine evolution. Chlorine generation was conducted with a 0.1 M NaCl (pH = 2) electrolyte, and the total chlorine concentration was determined by the DPD (N,N-diethyl-p-phenylenediamine) colorimetric method. In this method, DPD is oxidized to form a purple product by the reaction with chlorine, and the chlorine concentration was analyzed immediately using a spectrophotometer (DR/2010, HACH Co., Loveland, USA) at 530 nm [43]. The chlorine concentrations were replicated three times and the average values were obtained.

The stability of the prepared anodes was examined using the AST [12,44] with a current density considerably higher than that of industrial conditions. The time at which the potential of the anode escalates suddenly under chlorine evolution conditions was measured [45]. The experiments were performed galvanostatically at a current density of 1 A cm^{-2} in 5 M NaCl (pH = 2) at room temperature (25°C). The anode potential was recorded during the electrolysis.

3. Results and discussion

3.1. Surface analysis

3.1.1. Amount of deposited RuO_2

Fig. 1 shows the weights of the RuO_2 thin films deposited onto the Ti substrates according to the deposition time. As shown in Fig. 1, the weights of RuO_2 increase with the increase of the deposition time. The highest amount of RuO_2 (0.60 mg cm^{-2}) was deposited after 2.5 h. The deposited weight did not significantly increase with further deposition times to 3 h. A higher amount of RuO_2 was deposited than in a previous study [28]. This result could be due to the higher roughness of the etched Ti substrate compared with glass or stainless steel substrates. CBD can deposit well a thin film of RuO_2 nanoparticles onto the titanium substrate.

3.1.2. Morphology

Fig. 2 shows the SEM images of the RuO_2 electrodes with different deposition times. As shown in Fig. 2, the Ti substrates were well covered with RuO_2 nanoparticles. The roughness, porosity, and crack size increased as the deposition time was increased which is consistent with the increasing amount of RuO_2. It is expected that the total and outer surface area of the electrodes could be increased with the deposition time. The crack morphology is typical for DSA and advantageous for electrochemical chlorine evolution [46].

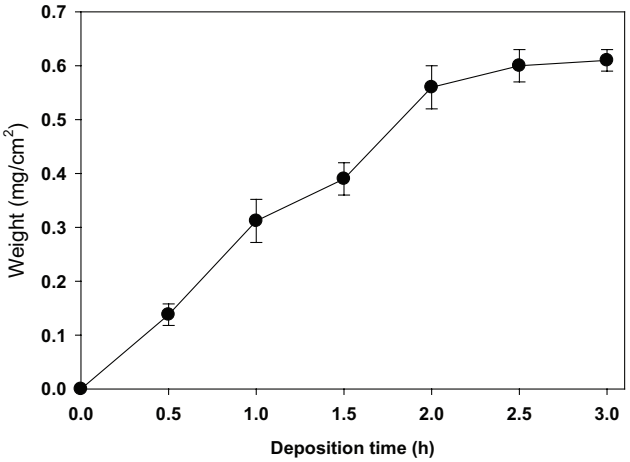

Fig. 1. Weights of the RuO_2 nanoparticles at different deposition times (0–3 h).

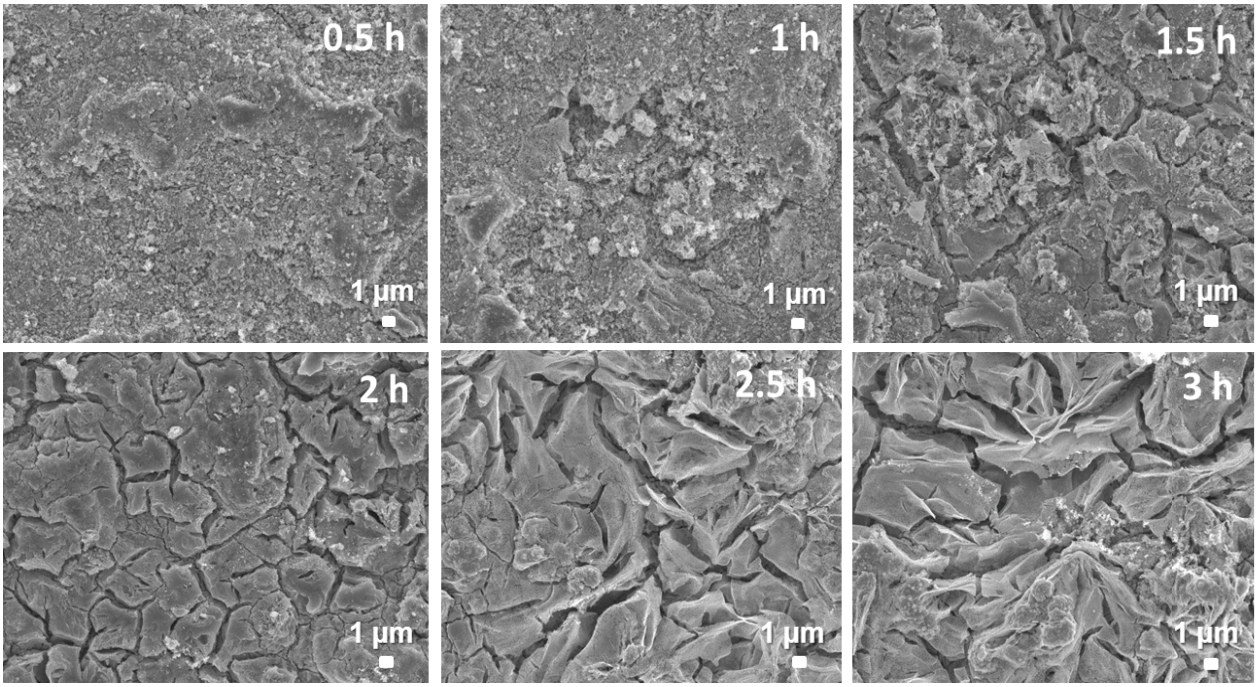

Fig. 2. SEM images of the RuO_2 electrodes with different deposition times (0–3 h).

3.1.3. Crystal pattern

Fig. 3 shows the high resolution scanning electron microscope (HRSEM) (a) and TEM (b) images of the RuO_2 nanoparticles deposited on the Ti substrate after a 2-h deposition. Spherical particles of RuO_2 and three-dimensional porous nanostructures were clearly seen in HRSEM. The average crystal size of the RuO_2 nanoparticles was 30 nm in diameter.

3.1.4. XRD spectra

Fig. 4 shows the XRD spectra of the RuO_2 electrodes made by the CBD route with different deposition times (1, 2, and 2.5 h). The XRD spectra suggest that the oxide nanoparticles in all cases are crystalline structures. The typical peaks of the rutile RuO_2 metal oxides were detected with high intensity of the 110 and 101 planes at about 28° and 35° for all of the electrodes. Because the catalyst layers were thin, the X-ray penetrated the coating layers and the Ti metal peak was detected. There was no detection of the ruthenium metallic phase, which is an undesirable phase for chlorine evolution while Ru metal was found in the electrodeposition method [15]. The intensity of the RuO_2 peaks from the diffraction profiles increases with increasing the deposition time, consistent with the amount of RuO_2 catalyst. CBD can deposit well polycrystalline RuO_2 nanoparticles onto the Ti substrates.

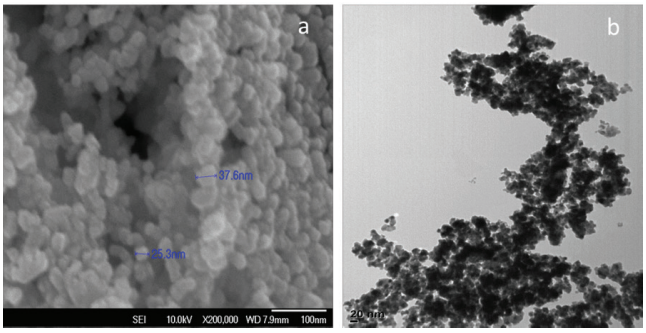

Fig. 3. HRSEM (a) and TEM (b) of the RuO_2 nanoparticles on the electrodes after a 2-h deposition.

3.2. Electrochemical analysis

3.2.1. Cyclic voltammetry and active surface area

Fig. 5 shows the CV at a scan rate of 320 mV/s (a) and voltammetric charge (b) of the RuO_2 electrodes at different deposition times (1, 2, and 2.5 h) in 0.5 M H_2SO_4. As shown in Fig. 5(a), all the CV curves are almost symmetrical to the zero potential line. Note that the rectangular shape of the CV of the RuO_2 electrodes remains unchanged with the scan rate, which indicates the good reversibility (redox reaction) of the system resulting from the insignificant iR (ohmic drop)

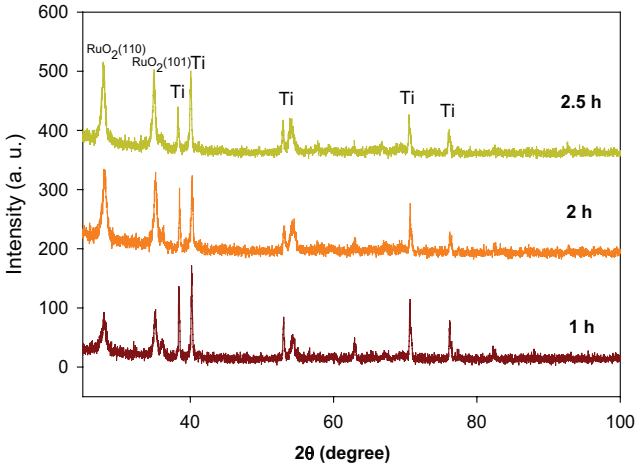

Fig. 4. XRD spectra of the RuO_2 electrodes with different deposition times (1, 2, and 2.5 h).

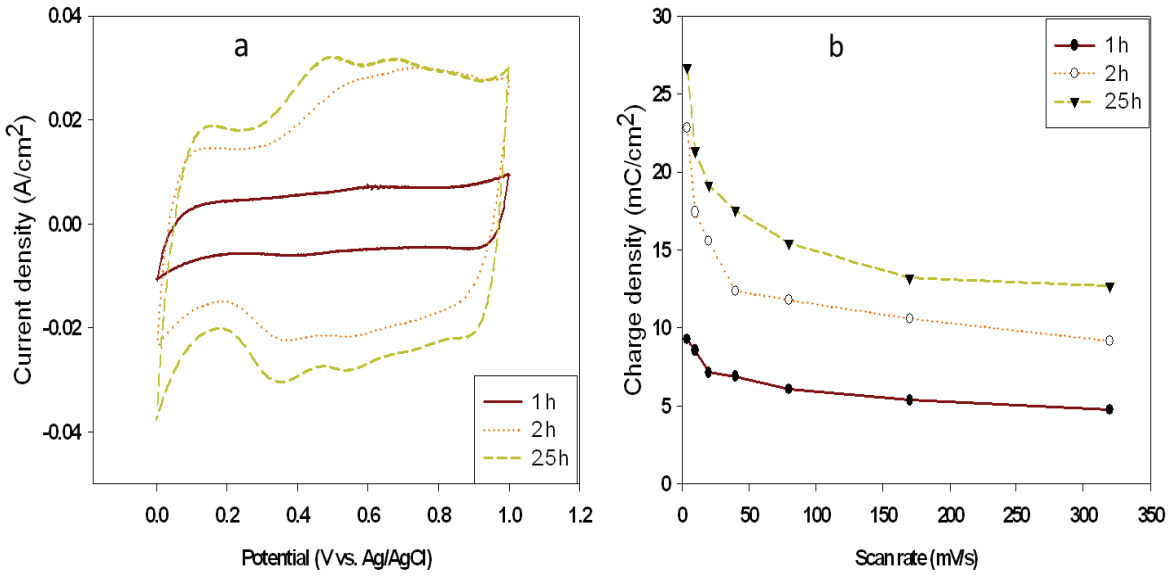

Fig. 5. CV at a scan rate of 320 mV/s (a) and voltammetric charge (b) of the RuO_2 electrodes with different deposition times (1, 2, and 2.5 h).

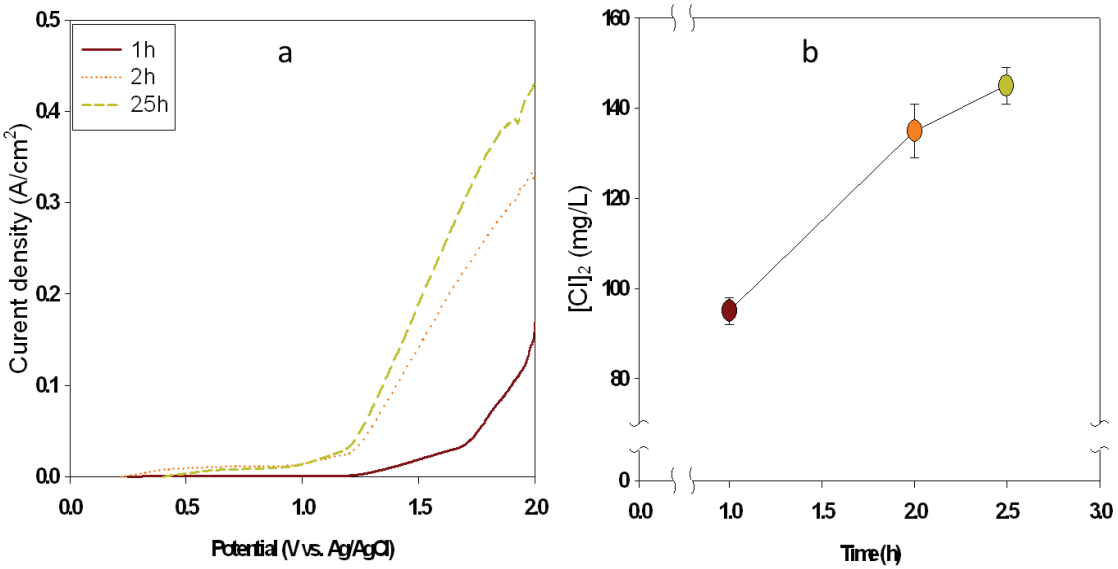

Fig. 6. LSV (a) and chlorine concentration (b) of the RuO_2 electrodes prepared at different deposition times (1, 2, and 2.5 h). Experimental conditions: (a) 5 M NaCl, pH = 2, (b) 0.1 M NaCl, pH = 2, t = 10 min.

loss. The current densities of the electrodes increase with the increase of the deposition time in the CVs.

The surface area (voltammetric charge) in Fig. 5(b) decreases with the increasing scan rate, which means that it is difficult for the electrolyte to penetrate the inner surface of the electrode. The total voltammetric charges of the electrodes deposited after 1, 2, and 2.5 h are 10.0, 24.9, and 28.1 mC/cm^2, while the outer voltammetric charges are 4.5, 9.0, and 12.7 mC/cm^2, respectively. The results show that the total and outer voltammetric charges increased with the deposition time. The explanation for this observation is the increase in the crack size with the increasing deposition time.

3.2.2. Chlorine evolution

Fig. 6 shows the LSV (a) and chlorine concentration (b) of the RuO_2 electrodes prepared at different deposition times (1, 2, and 2.5 h). As shown in Fig. 6(a), no reaction takes place at potentials below 1.17 V vs. Ag/AgCl. This behavior is expected because 1.17 V vs. Ag/AgCl represents the thermodynamic minimum potential for chlorine evolution under the studied conditions. However, potentials exceeding 1.17 V vs. Ag/AgCl cause a steady increase in the current density, which indicates chlorine and oxygen formation. The oxidation current is greatly influenced by the deposition time, while there is no apparent change in the onset potential of chlorine generation. The current density in Fig. 6(a) is supported by the chlorine concentration in Fig. 6(b). The current density and chlorine concentration increased with the increase of the deposition time. This order is consistent with the increased surface area of these electrodes (Fig. 5(b)). A previous study also suggested that chlorine evolution increases with an increase of the crack size [46].

3.2.3. Accelerated stability test

Fig. 7 shows the AST for the RuO_2 electrodes prepared with different deposition times (1, 2, and 2.5 h) for the CBD

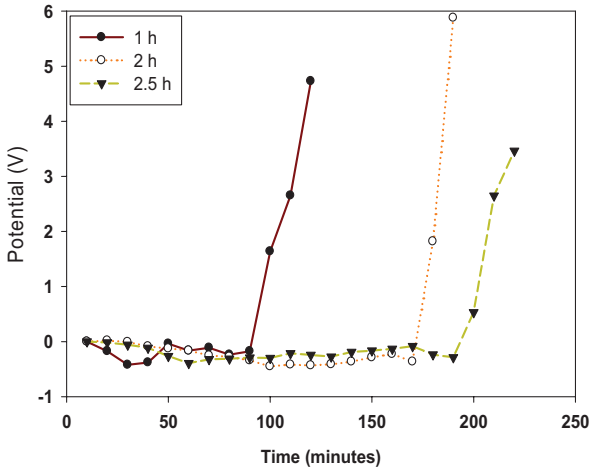

Fig. 7. The AST of the RuO_2 electrodes prepared at different deposition times (1, 2, and 2.5 h). Experimental conditions: 5 M NaCl, pH = 2, t = 25°C, I = 1 A cm^{-2}.

method. The lifetime of the RuO_2 electrodes increases with the deposition time under the same electrolysis condition. The electrode with a 1 h of deposition time has a lifetime of 90 min, while the lifetime of RuO_2 electrode with a 2 and 2.5 h deposition time is 170 and 190 min, respectively.

4. Conclusion

RuO_2 electrodes for chlorine evolution were successfully synthesized using the CBD method which is done in a single step, and is simple, easy, and efficient. The CBD method is useful for the preparation of large surface area RuO_2 electrodes with a rutile crystal structure, and a porous, crack morphology with an average grain size of 30 nm. The RuO_2 electrodes show a high electrocatalytic efficiency and stability for chlorine evolution. The amount of deposited RuO_2 as

well as the crack sizes, electrocatalytic activity and stability increased with the deposition time. CBD is an attractive synthesis route to fabricate promising RuO_2 electrodes for electrochemical chlorine evolution.

Acknowledgments

This research was supported by a grant (code 17IFIP-B065893-05) from Industrial Facilities & Infrastructure Research Program funded by Ministry of Land, Infrastructure and Transport of Korean government, and supported by Korea Ministry of Environment as "Global Top Project (E617-00211-0608-0)".

References

[1] H. Over, Surface chemistry of ruthenium dioxide in heterogeneous catalysis and electrocatalysis: from fundamental to applied research, Chem. Rev., 112 (2012) 3356–3426.
[2] T. Luu, C. Kim, S. Kim, J. Kim, J. Yoon, Fabricating macroporous RuO_2-TiO_2 electrodes using polystyrene templates for high chlorine evolution efficiencies, Desal. Wat. Treat., 77 (2017) 94–104.
[3] T. Luu, J. Kim, J. Yoon, A novel microwave-assisted synthesis of RuO_2-TiO_2 electrodes with improved chlorine and oxygen evolutions, Desal. Wat. Treat., 77 (2017) 105–111.
[4] X. Ma, Y. Gao, Y. Cui, H. Huang, J. Han, Electrochemical treatment of papermaking tobacco sheet wastewater on β-PbO_2 and Ti/TiO_2-RuO_2-IrO_2 electrodes, Desal. Wat. Treat., 57 (2016) 19557–19565.
[5] S. Trasatti, Electrocatalysis: understanding the success of DSA®, Electrochim. Acta, 45 (2000) 2377–2385.
[6] T. Luu, J. Kim, J. Yoon, Physicochemical properties of RuO_2 and IrO_2 electrodes affecting chlorine evolutions, J. Ind. Eng. Chem., 21 (2014) 400–404.
[7] T. Luu, J. Kim, C. Kim, S. Kim, J. Yoon, The effect of fabrication conditions of RuO_2 electrode to the chlorine electrocatalytic activity, Bull. Korean Chem. Soc., 36 (2015) 1411–1417.
[8] S. Trasatti, Electrocatalysis in the anodic evolution of oxygen and chlorine, Electrochim. Acta, 29 (1984) 1503–1512.
[9] H. Chen, H. Lai, J. Jow, Annealing effect on the performance of RuO_2–Ta_2O_5/Ti electrodes for use in supercapacitors, Mater. Chem. Phys., 125 (2011) 652–655.
[10] J. Kristof, J. Liszi, A. Battisti, A. Barbieri, P. Szabo, Thermoanalytical investigation of the formation of RuO_2-based mixed-oxide electrodes, Mater. Chem. Phys., 37 (1994) 23.
[11] C. Angejinetta, S. Trasatti, L. Atanasoska, Z. Minevski, Effect of preparation on the surface and electrocatalytic properties of RuO_2 + IrO_2 mixed oxide electrodes, Mater. Chem. Phys., 22 (1989) 231–247.
[12] V. Panic, A. Dekanski, M. Stankovic, S. Milonjic, B. Nikoli, On the deactivation mechanism of RuO_2–TiO_2/Ti anodes prepared by the sol–gel procedure, J. Electroanal. Chem., 579 (2005) 67.
[13] I. Kim, K. Kim, Electrochemical characterization of hydrous ruthenium oxide thin-film electrodes for electrochemical capacitor applications, J. Electrochem. Soc., 153 (2006) A383–A389.
[14] W. Shin, S. Yoon, Characterization of RuO_2 thin films prepared by hot-wall metallorganic chemical vapor deposition, J. Electrochem. Soc., 144 (1997) 1055–1060.
[15] C. Hu, C. Wang, T. Wu, K. Chang, Anodic composite deposition of hydrous RuO_2–TiO_2 nanocomposites for electrochemical capacitors, Electrochim. Acta, 85 (2012) 90–98.
[16] C. Lokhande, Chemical deposition of metal chalcogenide thin films, Mater. Chem. Phys., 27 (1991) 1–43.
[17] H. Pathan, C. Lokhande, Deposition of metal chalcogenide thin films by successive ionic layer adsorption and reaction (SILAR) method, Bull. Mater. Sci., 27 (2004) 85–111.
[18] R. Mane, C. Lokhande, Chemical deposition method for metal chalcogenide thin films, Mater. Chem. Phys., 65 (2000) 1–31.
[19] X. Xia, J. Tu, X. Wang, C. Gu, X. Zhao, Hierarchically porous NiO film grown by chemical bath deposition via a colloidal crystal template as an electrochemical pseudocapacitor material, J. Mater. Chem., 21 (2011) 671.
[20] C. Lokhande, A. More, J. Gunjakar, Microstructure dependent performance of chemically deposited nanocrystalline metal oxide thin films, J Alloys Compd., 486 (2009) 570–580.
[21] U. Patil, K. Gurava, O. Joo, C. Lokhande, Synthesis of photosensitive nanograined TiO_2 thin films by SILAR method, J. Alloys Compd., 478 (2009) 711–715.
[22] M. Suchea, S. Christoulakis, M. Katharakis, N. Vidakis, E. Koudoumas, Influence of thickness and growth temperature on the optical and electrical properties of ZnO thin films, Thin Solid Films, 515 (2006) 4303–4306.
[23] D. Dubal, A. Jagadale, S. Patil, C. Lokhande, Simple route for the synthesis of supercapacitive Co–Ni mixed hydroxide thin films, Mater. Res. Bull., 47 (2012) 1239–1245.
[24] R. Salunkhe, D. Dhawale, T. Gujar, C. Lokhande, Structural, electrical and optical studies of SILAR deposited cadmium oxide thin films: annealing effect, Mater. Res. Bull., 44 (2009) 364–368.
[25] X. Xia, J. Tu, Y. Zhang, X. Wang, C. Gu, X. Zhao, H. Fan, High-quality metal oxide core/shell nanowire arrays on conductive substrates for electrochemical energy storage, ACS Nano, 6 (2012) 5531–5538.
[26] S. Music, S. Popovic, M. Maljkovic, A. Saric, Synthesis and characterization of nanocrystalline RuO_2 powders, Mater. Lett., 58 (2004) 1431–1436.
[27] P. Deshmukh, S. Pusawale, A. Jagadale, C. Lokhande, Supercapacitive performance of hydrous ruthenium oxide (RuO_2·nH_2O) thin films deposited by SILAR method, J. Mater. Sci., 47 (2012) 1546.
[28] U. Patil, S. Kulkarni, V. Jamadade, C. Lokhande, Chemically synthesized hydrous RuO_2 thin films for supercapacitor application, J. Alloys Compd., 509 (2011) 1677.
[29] W. Lee, R. Mane, V. Todkar, S. Lee, O. Egorov, W. Chae, S. Han, Implication of liquid-phase deposited amorphous RuO_2 electrode for electrochemical supercapacitor, Electrochem. Solid-State Lett., 10 (2007) A225–A227.
[30] S. Pusawale, P. Deshmukh, J. Gunjakar, C. Lokhande, SnO_2–RuO_2 composite films by chemical deposition for supercapacitor application, Mater. Chem. Phys., 139 (2013) 416–422.
[31] V. Patake, C. Lokhande, Chemical synthesis of nano-porous ruthenium oxide (RuO_2) thin films for supercapacitor application, Appl. Surf. Sci., 254 (2008) 2820–2824.
[32] D. Dubal, G. Gund, R. Holze, H. Jadhav, C. Lokhande, C. Park, Solution-based binder-free synthetic approach of RuO_2 thin films for all solid state supercapacitors, Electrochim. Acta, 103 (2013) 103–109.
[33] S. Oh, L. Nazar, Direct synthesis of electroactive mesoporous hydrous crystalline RuO_2 templated by a cationic surfactant, J. Mater. Chem., 20 (2010) 3834–3839.
[34] X. Liu, X. Zhang, NiO-based composite electrode with RuO_2 for electrochemical capacitors, Electrochim. Acta, 49 (2004) 229–232.
[35] X. Fu, H. Yu, F. Peng, H. Wang, Y. Qian, Facile preparation of RuO_2/CNT catalyst by a homogenous oxidation precipitation method and its catalytic performance, Appl. Catal., A, 321 (2007) 190–197.
[36] R. Kotz, S. Stuck, Stabilization of RuO_2 by IrO_2 for anodic oxygen evolution in acid media, Electrochim. Acta, 31 (1986) 1311–1316.
[37] J. Jirkovsky, H. Hoffmannova, M. Klementova, P. Krtil, Particle size dependence of the electrocatalytic activity of nanocrystalline RuO_2 electrodes, J. Electrochem. Soc., 153 (2006) 111–118.
[38] C. Malmgren, A. Eriksson, A. Cornell, J. Backtrom, E. Eriksson, H. Olin, Nanocrystallinity in RuO_2 coatings—influence of precursor and preparation temperature, Thin Solid Films, 518 (2010) 3615–3618.
[39] H. Klug, H. Alexander, X-ray Diffraction Procedures, 2nd ed., Wiley, New York, 1974, p. 112.
[40] A. Bard, L. Faulkner, Electrochemical methods-Fundamentals and Applications, 2nd ed., Wiley, 2001, p. 200.

[41] P. Hong, N. Ngoc, D. Chi, L. Ba, Nanosized $Ir_xRu_{1-x}O_2$ electrocatalysts for oxygen evolution reaction in proton exchange membrane water electrolyzer, Adv. Nat. Sci.: Nanosci. Nanotechnol., 6 (2015) 025015.
[42] S. Ardizzone, G. Fregonara, S. Trasatti, "Inner" and "outer" active surface of RuO_2 electrodes, Electrochim. Acta, 35 (1990) 263–267.
[43] APHA, Standard Methods for the Examination of Water and Wastewater, 21st ed., American Public Health Association, Washington, D.C., 2005, p. 4.
[44] J. Ribeiro, A. Andrade, Characterization of $RuO_2Ta_2O_5$ coated titanium electrode microstructure, morphology, and electrochemical investigation, J. Electrochem. Soc., 151 (2004) 106–112.
[45] V. Panic, A. Dekanski, S. Milonjic, R. Atanasoski, B. Nikolic, The effect of the addition of colloidal iridium oxide into sol–gel obtained titanium and ruthenium oxide coatings on titanium on their electrochemical properties, Phys. Chem. Chem. Phys., 12 (2010) 7521–7528.
[46] A. Zeradjanin, F. Mantia, J. Masa, W. Schuhmann, Utilization of the catalyst layer of dimensionally stable anodes—interplay of morphology and active surface area, Electrochim. Acta, 82 (2012) 408–414.